Received 20 January 2025; revised 28 February 2025; accepted 3 March 2025. Date of publication 11 March 2025; date of current version 7 April 2025.

Digital Object Identifier 10.1109/OJCOMS.2025.3550308

Enabling Sub-Terahertz Broadband MIMO Communications With Leaky-Wave Antenna Arrays

ALBERT DIEZ-COMAS (Graduate Student Member, IEEE), DUSCHIA M. BODET (Graduate Student Member, IEEE), AND JOSEP M. JORNET (Fellow, IEEE)

Department of Electrical and Computer Engineering, Northeastern University, Boston, MA 02115, USA

CORRESPONDING AUTHOR: A. DIEZ-COMAS (e-mail: diezcomas.a@northeastern.edu)

This work was supported in part by NSF under Grant NSF-2211616 and Grant NSF-1954780, and in part by the Air Force Office of Scientific Research under Grant FA9550-22–1-0412.

ABSTRACT The increasing demand for high-speed wireless communications has led to the exploration of the terahertz (THz) band, where the broad available bandwidths promise significant data-rate improvements. However, propagation losses and the primarily line-of-sight (LoS) nature of THz channels present challenges for implementing spatial multiplexing in multiple-input multiple-output (MIMO) systems. In this paper, we propose a tilted leaky-wave antenna (LWA) array architecture to enable spatial multiplexing by leveraging the frequency-dependent beam-steering capabilities of LWAs. We present the first experimental implementation of a sub-THz, 2-element tilted LWA array. Our experimental results demonstrate that distinct data streams can be transmitted simultaneously with minimal interference. We also provide an analysis of the achievable data rates as a function of number of antennas and tilting angle, showing significant improvements under specific conditions. We further investigate the potential of a staircase LWA array in a multiuser scenario, showing that LWAs could be deployed in access points (APs) to exploit spatial multiplexing. In addition, we present a capacity comparison of different antenna array technologies. These findings establish the potential of tilted LWA arrays for future (sub-)THz MIMO systems, offering a practical approach to overcome the limitations of conventional spatial multiplexing techniques.

INDEX TERMS Leaky-wave antenna (LWA), communications, array, MIMO, spatial multiplexing, OFDM, sub-THz, THz.

I. INTRODUCTION

With the increasing demand for high-speed wireless communication applications, the terahertz (THz) band is being explored for its potential to enable high-speed links [1]. The broad available bandwidths at THz frequencies can provide the necessary spectrum for future communications. However, utilizing these frequencies for communications also comes with its own set of challenges, namely high propagation losses that lead to primarily line-of-sight (LoS) channels. Multiple-input multiple-output (MIMO) systems have been discussed extensively for THz communications for their ability to both enable beamforming gains to combat the high path losses and their potential to enable spatial multiplexing [2], [3], [4], [5], [6]. However, given the primarily LoS nature of the sub-THz and THz channels, (sub-)THz MIMO systems cannot rely on the multipath delay profile to enable spatial multiplexing in the same way that lower frequency MIMO systems can [7], [8]. Thus, determining methods to enable spatial multiplexing for MIMO systems is an important question.

Several approaches have been proposed to address the challenge of achieving MIMO spatial multiplexing at THz frequencies. These include optimizing antenna spacing based on the geometry of the MIMO system to create high-rank channel matrices [9], [10], employing an array-of-subarrays (AoSA) architecture [3], [11], [12], [13], and using antennas with different polarizations to enable the transmission of two orthogonal spatial channels [14]. Additionally, orbital angular momentum (OAM) is being investigated to generate orthogonal beams that propagate independently along the same axis by utilizing different OAM modes [15], [16]. Another technique involves leveraging the radiation patterns

of antenna elements to assist in forming orthogonal channels [17]. In this paper, we adopt the latter approach and explore the benefits of a sub-THz leaky-wave antenna (LWA) MIMO system.

LWAs have been used for communication and sensing applications due to their frequency-dependent beam-steering capabilities [18]. Recently, they have been investigated in the (sub-)THz frequency bands as a promising solution [1], particularly in light of the challenges at these frequencies, such as the immaturity and high cost of conventional beam-steering methods, which often require many phase shifters. Their frequency-dependent radiation pattern provides the necessary dynamism for communication systems without requiring mechanical reconfiguration or any electronic tunable component. In addition, LWAs are typically directive due to their elongated structure, which helps to reduce high path losses at (sub-)THz frequencies. Furthermore, the small wavelengths at these frequencies mean that even a physically large antenna remains relatively compact. For instance, our designed LWA for the 125-170 GHz frequency range is approximately 3 cm long, allowing for dense array configurations within a small area. However, LWAs are not without limitations: their frequency-dependent propagation direction constrains the usable bandwidth for a given beam direction.

While prior studies have examined the use of LWAs in single-input single-output (SISO) systems [19], [20] and for channel state information (CSI) estimation [21], [22], there has yet to be a presented architecture capable of enabling true spatial multiplexing in LWA MIMO systems. To address this gap, we introduce a novel array architecture, termed the tilted LWA array. This design leverages the unique properties of LWAs to achieve angular spatial multiplexing by tilting the array elements consecutively and utilizing their frequency-dependent beam-steering capabilities to ensure that radiated beams remain non-interfering across all frequencies. This innovative approach enhances achievable data rates and significantly improves effective bandwidth, positioning it as a compelling solution for overcoming the challenges inherent to (sub-)THz MIMO communications.

This work is an extension of our previous work in [23], and the contributions of the paper are:

1) We propose a novel array architecture for LWAs, referred to as the tilted LWA array, which enables spatial multiplexing with angular resolution and minimal interference. We further extend this design to cover the full 360° angular range for multiuser scenarios, naming it the staircase LWA array.
2) We develop a system model to facilitate a detailed comparison of achievable data rates between combining and spatial multiplexing using tilted LWA arrays in 2×2 and 16×16 MIMO configurations. The comparison is evaluated for different tilting angles and transmission distances to identify the conditions under which spatial multiplexing performs better than combining. In addition, we analyze the data rates achieved with a staircase LWA array in a multiuser scenario, considering different numbers of transmitters and receivers, and demonstrate how LWAs can enable high data rates in such scenarios. Finally, we compare the performance of the tilted LWA array with other antenna array architectures, highlighting the situations where an LWA array is most advantageous and discussing its tradeoffs relative to existing solutions.
3) We present and experimentally validate a sub-THz LWA design that consists of a rectangular waveguide with a longitudinal slit, providing 20° steerability and a gain between 12 dBi and 18 dBi when operating in the 125 GHz and 170 GHz range.
4) We experimentally validate the performance of a broadband tilted LWA MIMO system in the sub-THz band by sending and demodulating information-bearing signals from a 2-element tilted LWA at 147.5 GHz. The results indicate that the tilted LWA array can increase the effective data rate through spatial multiplexing for certain angular separations.

The findings presented in this paper highlight the substantial capacity gains achieved with tilted LWA arrays, which were demonstrated both theoretically and experimentally. Our work underscores the advantages of utilizing LWAs in the (sub-)THz region, particularly for high-capacity, practical implementations.

The rest of this paper is organized as follows. Section II presents the related works. In Section III, we describe the system model used for the numerical analysis and present the corresponding results in Section IV. Section V presents the experimental validation of the designed LWA and the MIMO techniques implemented in the proposed tilted LWA array. Section VI discusses the challenges and future research directions. Finally, Section VII concludes the paper.

II. RELATED WORK

This section delves into related work in (sub-)THz technologies, beginning with a discussion of state-of-the-art antennas, including reconfigurable antenna systems and reconfigurable intelligent surfaces (RIS). Next, we examine advances in LWAs designed for these frequencies. Finally, we explore the progress made in (sub-)THz MIMO systems, focusing on techniques that enable spatial multiplexing.

A. (SUB-)THZ ANTENNAS AND RECONFIGURABLE ANTENNAS

Recent research has demonstrated significant advancements in antenna technologies for (sub-)THz wireless communications. For example, [24] provides an extensive review of critical components, including antennas, RIS, and reconfigurable antenna systems, offering a current perspective on state-of-the-art solutions. Among these innovations, [25] shows a significant progress, demonstrating an electronically steerable pencil beam operating at 265 GHz. The system features a 98×98 element array controlled by complementary

metal-oxide-semiconductor (CMOS) microelectronic chips and achieves a ±60° steering range in both azimuth and elevation, with a 1° beamwidth corresponding to a 42 dBi directivity, though total losses result in a gain of 12 dBi.

In another advancement, [26] presents a programmable metasurface operating at 300 GHz, using CMOS-based split-ring resonators with 84 distinct states per unit cell. This metasurface achieves ±30° beam steering and a 25 dB amplitude modulation depth. Similarly, [27] explores a graphene-based reflectarray metasurface at 1 THz, achieving a steering range of 25° in one direction and showcasing the potential of novel materials in this domain.

At lower frequencies, [28] and [29] demonstrate RIS implementations at microwave and millimeter-wave bands, respectively, highlighting notable progress in their practical deployment for wireless systems. Beyond RIS, advancements in phased-array transmitter technology, such as the system described in [30], have also been reported. Operating between 370 and 410 GHz, this transmitter achieves a peak effective isotropic radiated power (EIRP) of 8–8.5 dBm and provides ±35° beam steering in a single plane.

Lens antennas have also gained attention for their ability to enhance directivity and focus radiation. A noteworthy example is presented in [31], which describes an integrated Luneburg and Maxwell fish-eye lens system operating at 330 GHz. This design produces collimated beams over a ±60° range with gains of 18–20 dBi, further emphasizing the potential of lens-based solutions in sub-THz applications.

The rapid evolution of (sub-)THz hardware has significantly advanced the development of more robust and efficient wireless communications. However, despite the considerable progress, several challenges remain. One major issue is that the dynamic performance of reconfigurable reflectarrays and antennas comes at the cost of narrow bandwidth. This limitation arises from their reliance on resonant elements that function effectively only within a narrow frequency range. Additionally, at sub-THz and THz frequencies, reflectarrays and RIS face efficiency and fabrication difficulties due to increased material losses, parasitic effects, and challenges in precisely controlling high-frequency components at such small scales.

B. (SUB-)THZ LEAKY-WAVE ANTENNAS

Due to their ability to beam-steer without the need for complex feeding systems, LWAs have garnered significant attention at THz frequencies. Various studies have explored different LWA designs. Notably, LWAs utilizing parallel-plate waveguides have been extensively investigated at (sub-)THz frequencies [19], [32], [33], primarily because of their ease of manufacturing and straightforward coupling from free-space beams. A longitudinal slit is introduced in one of the plates, through which the beam leaks to free-space at specific angles, characteristic of LWA behavior. However, the use of parallel plates poses challenges in confining electromagnetic (EM) waves within the waveguide, often leading to high losses. To address this, a conventional LWA using a rectangular waveguide can be used, as in [34].

Additionally, LWAs based on microstrip lines have also been developed in the (sub-)THz region, as demonstrated in [20], [35], [36]. These designs enable LWA integration on printed circuit boards (PCBs) or substrates, offering compact, lightweight, and easily fabricated solutions. At lower frequencies, many LWAs of this type have been developed with electronic reconfiguration achieved by applying a voltage bias to components like PIN diodes or varactors, which allows beam steering without altering the operating frequency. However, such reconfigurability has yet to be fully realized at THz frequencies. Recent research efforts have theoretically explored the use of advanced materials, such as graphene [37], [38], [39], despite its complex fabrication process, and liquid crystals [40], but it still lacks an experimental validation.

C. ENABLING SPATIAL MULTIPLEXING IN THE (SUB-)THZ REGIME

There have been numerous works exploring (sub-)THz MIMO. Given the primarily LoS nature of the channel there have been a number of solutions put forward to enable spatial multiplexing in the (sub-)THz regime. Perhaps most notable, the AoSA architecture was proposed in [3] and [11] to enable multiplexing for (sub-)THz systems. The array architecture is designed to enable different streams to be transmitted on a different subarray. In theory, these architectures are effective and many papers have been written explaining how the AoSA architecture could be implemented [41], [42], [43]. However, to our knowledge, there have only been two works in the past decade that have come close to achieving the AoSA architecture in practice [12], [13], and even these works do not exhibit spatial multiplexing. There are many challenges that make the AoSA architecture difficult to fabricate in practice including the small apertures and the need for proper power supply and cooling techniques in such a confined area.

Another approach to enabling spatial multiplexing in (sub-)THz LoS channels is to engineer the inter-element spacing of antenna arrays based on geometry that maximizes channel capacity [9], [10]. Given that multipath effects are negligible in (sub-)THz LoS channels, maximizing capacity involves ensuring that each spatial path is as independent as possible. This is achieved by optimizing the geometric arrangement of the antenna elements to maximize the mutual orthogonality of the channels, thus effectively enabling spatial multiplexing. However, this method requires detailed knowledge of the channel characteristics and should be capable of mechanical reconfiguration if channel conditions change, which can complicate its implementation in dynamic scenarios.

Other methods to achieve spatial multiplexing include using antennas with different polarizations to transmit orthogonal channels–one horizontally polarized and the other vertically polarized [14]. Additionally, multiple co-propagating beams can be multiplexed using

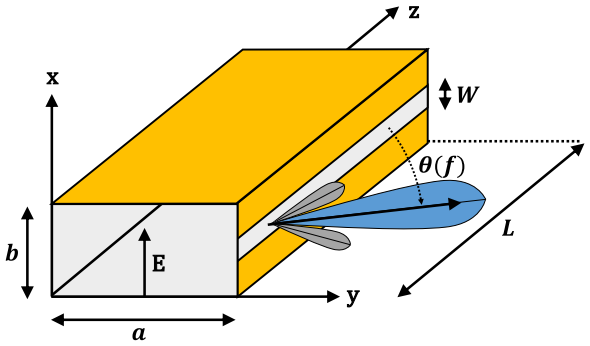

FIGURE 1. Geometry of the rectangular waveguide LWA and its parameters.

OAM [15], [16]. The principle here is that multiple data streams can be transmitted using different OAM modes, as these modes are orthogonal to each other and can be demultiplexed at the receiver.

Finally, directional antennas have been proposed for (sub-)THz MIMO systems [17]. Their high directivity helps mitigate propagation losses and can also enable spatial multiplexing by generating orthogonal channels through their characteristic radiation patterns. This approach can be viewed as each directional antenna functioning as a subarray in an AoSA architecture. This method simplifies the hardware complexity of the system, but the authors of [17] only consider a planar array of horn antennas in their analysis.

In addition to these methods, a MIMO wireless system utilizing dynamic radiation pattern diversity through composite right/left-handed (CRLH) LWAs has been proposed [44]. This system offers significant flexibility due to the electronically reconfigurable LWAs (not yet implemented at THz frequencies), which can produce a variety of radiation patterns. However, the primary goal of this system is to enhance reliability by leveraging these diverse radiation patterns rather than achieving spatial multiplexing.

Based on this analysis, it is clear that much research is being conducted in (sub-)THz MIMO systems. However, there are still many challenges to achieve spatial multiplexing on (sub-)THz systems. Notably, the existing works are either hardware-intensive or lack the reconfigurability necessary for modern communication systems. In this work, we demonstrate that the proposed tilted LWA array can achieve spatial multiplexing with angular resolution without the need for complex feeding systems, leveraging its frequency-dependent radiation pattern to do so, which can enable the high data rates required by next-generation communication systems.

III. SYSTEM MODEL

In this analysis, we consider the rectangular waveguide LWA shown in Figure 1. The figure illustrates the behavior of the LWA. Within the waveguide, a traveling wave in the fundamental mode exhibits an electric field distribution characteristic of the TE10 mode, with its polarization represented by vector E. Energy is "leaked" into free-space through a slit in the narrow side of the waveguide, with the direction of propagation determined by the operating frequency. We selected this type of LWA for its simplicity, efficiency, and its ability to provide a general understanding of the proposed system. Nonetheless, the insights presented in this paper are applicable to other LWA designs.

Operating in its fundamental mode, the rectangular waveguide LWA radiates solely in the forward direction, and its normalized far-field pattern of the LWA can be calculated by treating the slit as a magnetic dipole. The far-field LWA gain is given by

$$G_{\text{LWA}} = \text{sinc}^2\left[\frac{L}{2}(k_z - k_0\cos\theta)\right], \tag{1}$$

where $\text{sinc}(x) = \sin(x)/x$, L is the effective length of the slit, $k_z = \alpha - j\beta$ is the complex wavenumber vector, with α and β being the attenuation factor and propagation vector, respectively. k_0 is the free-space wavenumber and θ is the elevation angle.

From (1), the angle where the beam maximum is located can be predicted by

$$\theta = \cos^{-1}\left(\frac{\beta}{k_0}\right), \tag{2}$$

for $0 < \beta < k_0$, which is known as the fast-wave mode, the regime where it can radiate energy into free space. For the LWA operating in its fundamental mode, the propagation constant in an empty rectangular waveguide is

$$\beta = k_0\sqrt{1 - \left(\frac{c}{2af}\right)^2} = k_0\sqrt{1 - \left(\frac{f_{c,10}}{f}\right)^2}, \tag{3}$$

where c is the speed of light in free space, a is the waveguide width, f is the operating frequency, and $f_{c,10} = c/2a$ is the cutoff frequency at the fundamental mode TE10.

The LWA radiates in the forward direction (i.e., to $z > 0$). At the cuttoff frequency ($\beta = 0$), the LWA radiates towards the broadside direction (y-axis). As the frequency increases, the radiation direction shifts asymptotically toward the end-fire direction (z-axis). We refer to the scanning plane, or elevation plane, as the YZ plane. The cross-plane, or azimuth plane, is defined as the plane of constant value θ, perpendicular to the scanning plane, and intersecting the point of maximum beam intensity.

A. SCENARIO

We utilize a tilted array of LWAs to generate orthogonal channels, enabling spatial multiplexing. The principle behind this is represented in Figure 2. Each LWA primarily directs its beam according to the angle specified in (2), which varies with frequency. Thus, the total operating bandwidth can be divided into several subbands, with each subband radiating towards a different angular range. In a tilted structure, each LWA in the array transmits in a different direction for a specific frequency. As long as the tilt angle is greater than the beamwidth, each LWA can transmit independent data streams across the entire bandwidth with minimal

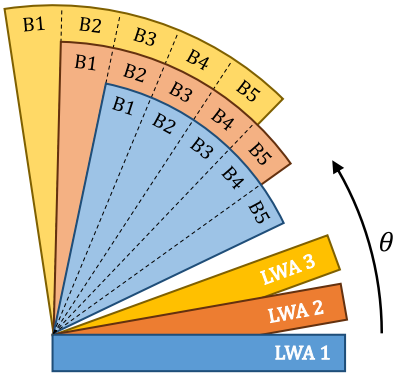

FIGURE 2. Representation of spatial multiplexing using a tilted LWA array.

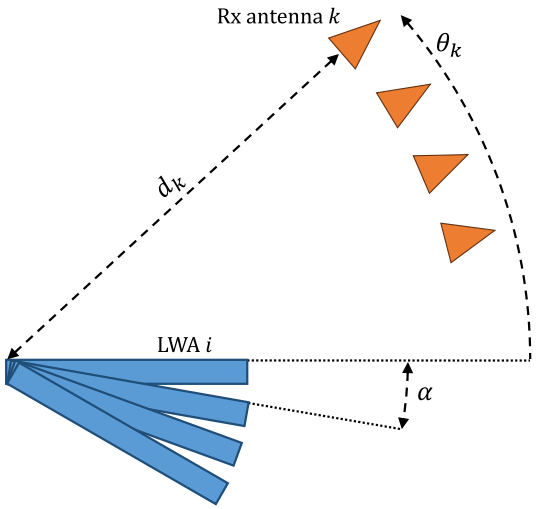

FIGURE 3. MIMO system model with a tilted LWA array.

interference between each other. Moreover, this architecture allows multiple LWAs to transmit in the same direction, each utilizing a different subband. This effectively increases the usable bandwidth directed towards a particular angle, thereby overcoming previous bandwidth limitations of LWA arrays and enhancing their performance in communication systems. It is important to note that the usable bandwidth of the array is also influenced by the performance of each LWA element and the tilting angle between the antenna elements. In general, a more directive LWA tends to restrict the range of frequencies that can effectively be transmitted in a given direction. Therefore, careful design of both the individual LWAs and the overall tilted array is essential to ensure optimal performance.

We develop a scenario to study the performance of the tilted LWA array. Figure 3 shows an $N_T \times N_R$ MIMO system, where the transmit antennas consist of LWAs. Each LWA in the array is tilted by an angle α relative to its neighboring element in the scanning plane. For simplicity, we assume that the LWAs lie in the same plane. The receive antennas consist of arbitrary antenna types and are oriented toward the transmitter at a distance d_k and an angle θ_k.

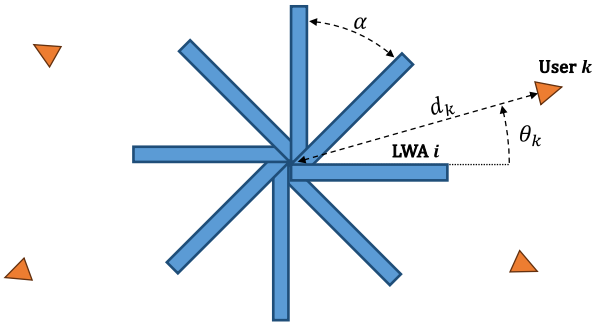

FIGURE 4. Multiuser system model with a staircase LWA array.

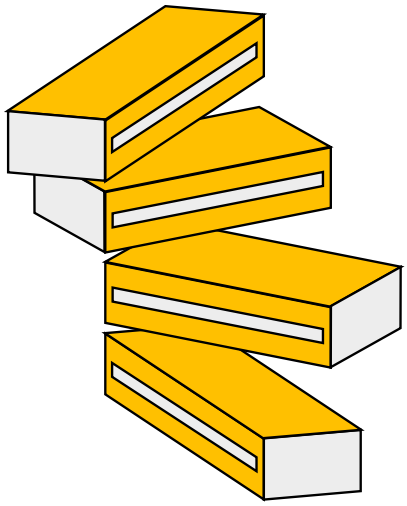

FIGURE 5. Geometry of the staircase LWA array architecture.

We extend this tilted array design to a multiuser scenario by uniformly distributing angularly the LWAs on the transmitter side to cover the full 360° range, as illustrated in Figure 4. The tilting angle is set to $\alpha = 360°/N_T$, forming an access point (AP) made up of LWAs. We refer to this structure as the staircase LWA array, as the LWAs are stacked vertically and tilted like steps in a staircase, as shown in Figure 5. In this scenario, we consider single-antenna users in the downlink. The base station is assumed to have knowledge of at least the amplitude of the channel response for each user. We do not assume user cooperation in this setup, meaning successive interference cancellation (SIC) is not performed. However, multiple LWAs can transmit to a single user, with the signals being combined at the receiver. As before, the users are oriented toward the transmitter, each positioned at a distance d_k and an angle θ_k.

B. CALCULATING CAPACITY AND ACHIEVABLE DATA RATES

To analyze the performance of the previous scenario, we define the capacity of the MIMO system and the theoretical data rates when performing combining and spatial multiplexing. We consider a channel response that accounts for the spherical propagation of waves. However, to include the effect of the LWAs, we incorporate the radiation

pattern of both transmit and receive antennas in the study. Furthermore, we consider a wide bandwidth to account for the frequency-selective channel. From these considerations, the channel response between transmitter i and receiver k can be defined as

$$h_{k,i}(f) = \alpha\big(d_{k,i}, f\big)\sqrt{G_{T,k,i}G_{R,k,i}}e^{-j2\pi f/c_0 d_{k,i}}, \tag{4}$$

where c_0 is the speed of light, f is the operating frequency, $d_{k,i}$ is the distance between each antenna pairs. $\alpha(d_{k,i}, f) = c_0/4\pi f d_{k,i}$ is the propagation loss characterized by the spreading loss, $G_{T,k,i}$ and $G_{R,k,i}$ are the gains of the transmit and receive antennas, respectively. With these definitions, the channel matrix takes the form

$$H = \begin{bmatrix} h_{1,1} & h_{1,2} & \cdots & h_{1,N_T-1} & h_{1,N_T} \\ h_{2,1} & h_{2,2} & \cdots & h_{2,N_T-1} & h_{2,N_T} \\ \cdot & \cdot & & \cdot & \cdot \\ \cdot & \cdot & & \cdot & \cdot \\ \cdot & \cdot & & \cdot & \cdot \\ h_{N_R-1,1} & h_{N_R-1,2} & \cdots & h_{N_R-1,N_T-1} & h_{N_R-1,N_T} \\ h_{N_R,1} & h_{N_R,2} & \cdots & h_{N_R,N_T-1} & h_{N_R,N_T} \end{bmatrix}. \tag{5}$$

The capacity of a frequency-selective MIMO system can be calculated by dividing the bandwidth into multiple subbands, such that each can be considered frequency-flat within each subband. Assuming channel state information at the transmitter, singular value decomposition (SVD) can be applied to identify the different eigenchannels and their respective eigenvalues, and the waterfilling algorithm [45] can be applied to the different eigenchannels and frequencies. The capacity results in

$$C = \frac{B}{M}\sum_{m=1}^{M}\sum_{i=1}^{N_{min}}\log\left(1 + \frac{P_i^m\big(\lambda_i^m\big)^2}{N_0 B/M}\right), \tag{6}$$

where B is total bandwidth, M is the number of sub-bands, and N_{min} is the rank of H, or equivalently its number of non-zero singular values. P_i^m and λ_i^m are the water-filling power allocations and singular values of H, respectively, for a eigenchannel i and in the subband m. N_0 is the noise spectral density.

The transmit power is allocated over the different eigenchannels and sub-bands following the waterfilling algorithm

$$P_i^m = \left(\mu - \frac{N_0 B}{M\big(\lambda_i^m\big)^2}\right)^+, \tag{7}$$

where $(x)^+$ denotes $\max(0, x)$, and μ is the water level, which is chosen such that the total power constraint is satisfied

$$\sum_{m=1}^{M}\sum_{i=1}^{N_{min}} P_i^m = P, \tag{8}$$

where P is the total transmit power.

For the theoretical data rate when performing combining or using another spatial diversity scheme, such as the Alamouti scheme we use in our experimental analysis, we can define the SNR of the system at a subband m as the combined signals over the multiple channels

$$\gamma_{SD}^m = \frac{\sum_{i=1}^{N_T}\sum_{k=1}^{N_R} P_{k,i}^m\left|h_{k,i}^m\right|^2}{N_0 B/M}, \tag{9}$$

where the power allocation at each transmitter i is now calculated as

$$P_i^m = \left(\mu - \frac{N_0 B}{M\sum_{k=1}^{N_R}|h_{k,i}|^2}\right)^+, \tag{10}$$

with a similar power constraint as before

$$\sum_{m=1}^{M}\sum_{i=1}^{N_T} P_i^m = P. \tag{11}$$

Then, the total SNR can be calculated as

$$\gamma_{SD} = \sum_{m=1}^{M}\gamma_{SD}^m, \tag{12}$$

and the theoretical data rate results in

$$R_{SD} = \frac{B}{M}\sum_{m=1}^{M}\log(1 + \gamma_{SD}). \tag{13}$$

In the spatial multiplexing case, we want to transmit different data streams to each receiver. The procedure we propose is as follows. First, each transmit antenna selects the best receiver to send the signal to in every subband. If multiple transmit antennas want to send to a single receive antenna, they send the same data signal, and the receive antenna combines the received signal. However, the signals from the transmit antennas that are received by non-intended receive antennas will be treated as interference. The SINR at a receive antenna k and subband m can be calculated as

$$\gamma_{SM,k}^m = \frac{\sum_{i=1}^{N_T} P_{k,i}^m|h_{k,i}^m|^2}{N_0 B/M + \sum_{i=1}^{N_T}\sum_{\substack{j=1\\ j\neq k}}^{N_R} P_{j,i}^m|h_{k,i}^m|^2}, \tag{14}$$

where the power allocation is performed at each transmitter selecting the best receiver

$$P_i^m = \left(\mu - \frac{N_0 B}{M\max\limits_k |h_{k,i}|^2}\right)^+, \tag{15}$$

with the same power constraint as in (11). The theoretical data rate for this method is calculated as

$$R_{SM} = \frac{B}{M}\sum_{m=1}^{M}\sum_{k=1}^{N_R}\log\big(1 + \gamma_{SM,k}^m\big). \tag{16}$$

These theoretical data rates are valuable for assessing the practical performance of the tilted LWA array. Thus, in addition to calculating the theoretical capacity of the system, we also provide these achievable rates for practical implementations.

Finally, we provide the capacity expression for a MISO system, as it will be utilized in the numerical results presented in Section IV-B. The capacity of the MISO system is given by

$$C = \frac{B}{M}\sum_{m=1}^{M}\log\left(1+\frac{\sum_{i=1}^{N_T} P_i^m |h_i^m|^2}{N_0 B/M}\right), \tag{17}$$

with the power allocation defined as

$$P_i^m = \left(\mu - \frac{N_0 B}{M|h_i^m|^2}\right)^+, \tag{18}$$

and the same total power constraint provided in (11).

IV. NUMERICAL ANALYSIS

In this section, we present a numerical analysis of the performance of the proposed LWA arrays. First, we conduct a numerical study to analyze the capacity and theoretical data rates achievable with LWA arrays under different configurations. Next, we compare the capacity of a MISO system achievable across an area using the tilted LWA array with that of an array of directional antennas and a beamforming phased array.

A. DATA RATE ANALYSIS OF LEAKY-WAVE ANTENNA ARRAYS

The performance of the MIMO systems described in Section III-A is evaluated. Figure 6 and Figure 7 show the capacities and data rates as a function of distance for a 2×2 and 16×16 MIMO configurations, respectively, for the system model shown in Figure 3. The capacity and data rates for combining and spatial multiplexing are calculated using (6), (13), and (16), respectively. The plots show the results for different tilting angles, α, between the transmitting LWAs, 0°, 10°, and 20°. This way, we can see the spatial multiplexing capabilities as the tilt increases and compare it with the non-tilted LWA array. All N_R receive antennas are allocated at the same distance $d = 1$ m. They are uniformly angularly separated, with an angular separation equal to the angle tilt. The first receive antenna starts at $\theta_1 = 45°$, and the neighboring ones are separated angularly by α. Hence, the relative angle between each pair of LWA i and Rx antenna i is equal. For example, for the case with $\alpha = 10°$, the Rx antenna angles would be 45°, 35°, 25°, ...The LWA gains are calculated from (1) and scaled to match the gains obtained from simulations, shown in Figure 13. The receive antennas gain are set to 21 dBi. The frequency range is between 120 GHz and 170 GHz, and this 50 GHz bandwidth is divided into $M = 50$ subbands. The total transmit power and the noise spectral density are $P_T = 13$ dBm and $N_0 = 1.9 \times 10^{-17}$ W/Hz, respectively. The analysis was conducted using parameters similar to those in our lab setup to provide an overview of the expected performance in practical real-world scenarios.

The results follow what we would expect. We see how for both 2×2 and 16×16 cases, spatial multiplexing with the tilted LWA array shows better performance at close distances, where the SNR is higher, while combining with the non-tilted LWA array shows better performance after a certain distance, for which the SNR is not high enough for the channel to enable spatial multiplexing. This tradeoff between combining and spatial multiplexing is well documented in the literature, where combining offers improved reliability in low SNR regimes, while spatial multiplexing provides higher data rates in high SNR conditions.

This analysis using 2×2 and 16×16 MIMO configurations illustrates the scalability of spatial multiplexing as the number of LWAs increases. When the array is tilted, the theoretical spatial multiplexing data rate approaches the capacity, whereas the combining rate lags behind. Conversely, in the non-tilted array, combining closely matches the capacity, and spatial multiplexing falls behind. Finally, it can be seen that a tilt of 10° performs better than 20° in the tilted LWA array. Although a higher tilt allows for better selectivity and the spatial multiplexing capabilities increase (as will be shown later in the experimental results), it reduces the number of receivers within each LWA's scanning range, decreasing overall capacity. This study demonstrates that selecting an appropriate tilt angle is essential and must be based on the LWA radiation pattern and system parameters.

We next evaluate the theoretical performance of the staircase LWA array in a multiuser scenario, illustrated in Figure 4. To simulate a multiuser scenario in a small cell area, receivers are randomly allocated in a uniform distribution at any angle and at distances between $d_{min} = 1$ m and $d_{max} = 10$ m. In this analysis, we only calculate the theoretical data rate for spatial multiplexing. Since no user cooperation is assumed, the MIMO capacity and receiver combining does not make sense here, so we focus in determining the achievable data rates in a multiuser scenario with the proposed spatial multiplexing method, shown in (16). The total power at the AP is set to $P_T = 30$ dBm, which is typical in localized wireless networks such as Wi-Fi, and the receive antenna gains to 3 dBi. We perform $N = 1000$ simulations and calculate the average sum data rates.

Figure 8 illustrates the data rates for spatial multiplexing from (16) for varying numbers of transmit antennas and users. The plot shows that data rates generally increase with the number of transmit or receive antennas. Increasing the number of receivers enhances diversity and spectral efficiency. Similarly, adding more transmit antennas is beneficial until interference between adjacent antennas limits performance. Hence, there is a maximum number of transmit antennas beyond which capacity no longer increases. This occurs when the angular separation between transmit antennas is smaller than the beamwidth, preventing the transmission of more independent data streams and reaching the spectral efficiency limit.

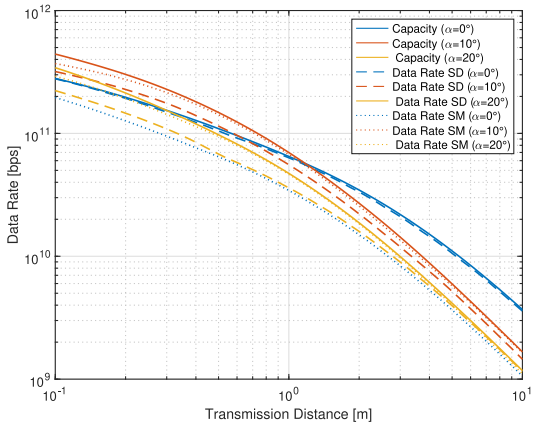

FIGURE 6. Capacity and theoretical data rates for spatial diversity (SD) and spatial multiplexing (SM) in a 2×2 MIMO system as a function of transmission distance, shown for different tilting angles.

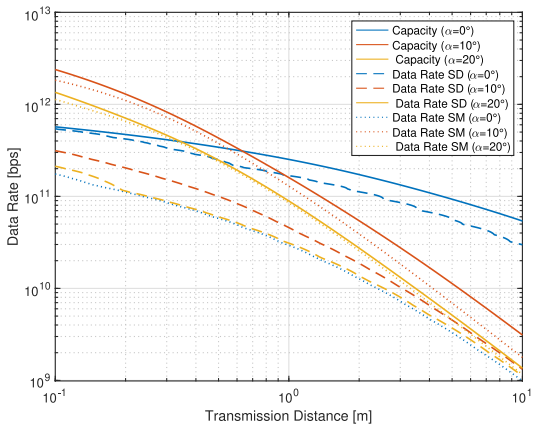

FIGURE 7. Capacity and theoretical data rates for spatial diversity (SD) and spatial multiplexing (SM) in a 16×16 MIMO system as a function of transmission distance, shown for different tilting angles.

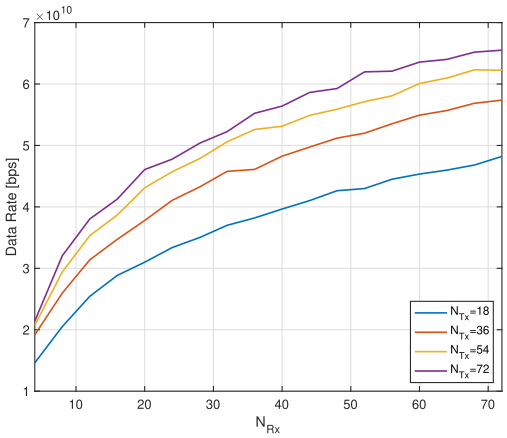

FIGURE 8. Theoretical data rates for spatial multiplexing in multiuser MIMO for different numbers of transmitters and receivers.

B. CAPACITY COMPARISON ACROSS DIFFERENT ARRAY ARCHITECTURES

The performance of the tilted LWA array is evaluated against other array architectures discussed in Section II-C,

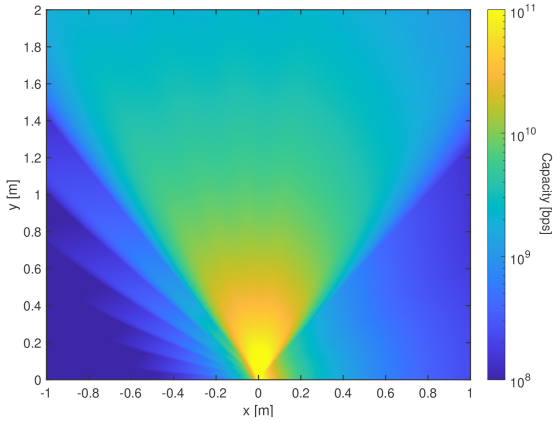

FIGURE 9. Achievable capacity of a tilted LWA array transmitter with a tilting angle of 10° across an area in a 4×1 MISO system.

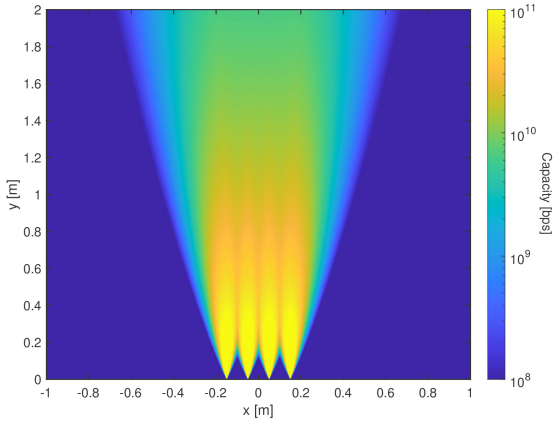

FIGURE 10. Achievable capacity of a horn antenna array transmitter across an area in a 4×1 MISO system.

specifically an array of horn antennas and a beamforming phased array composed of patch antennas. The array of horn antennas provides a relevant comparison, as horn antennas are widely used in (sub-)THz systems due to their high directivity. In contrast, the beamforming phased array exemplifies the AoSA approach, which typically employs patch antennas with beamforming capabilities.

To assess performance, the capacity of a 4×1 MISO system from (17) is measured over a defined area to illustrate the coverage provided by each architecture. Figure 9 illustrates the capacity over an area using the tilted LWA array with a tilting angle of $\alpha = 10°$. The same LWA properties as described in the previous section are applied. Each point on the plot represents the capacity at that specific position. The LWAs are used as transmit antennas, and the single receiver has a gain of 3 dB. The total transmit power is set to $P_T = 13$ dBm.

Figure 10 presents the results for an array of horn antennas with a gain of 21 dBi. The horn antennas are arranged in a uniform linear array (ULA) configuration with a separation of 10 cm, a common setup for combining. The gain of the

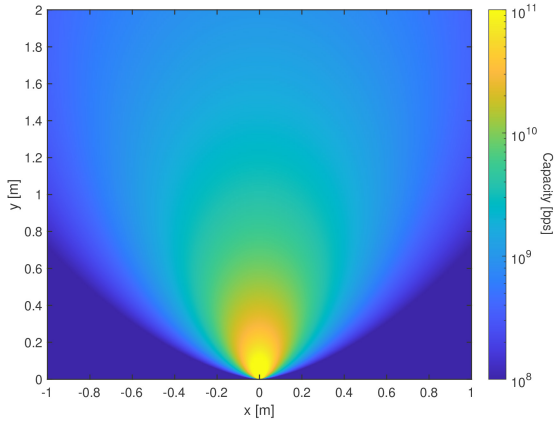

FIGURE 11. Achievable capacity of a beamforming patch antenna array transmitter across an area in a 4×1 MISO system.

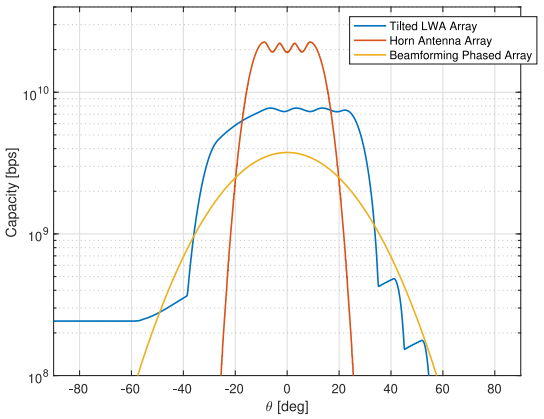

FIGURE 12. Achievable capacity at a distance of 1 m as a function of the propagation angle.

horn antennas is modeled with a Gaussian function

$$G_{\text{Horn}} = G_0 \exp\left(-\theta/\theta_0\right)^2, \tag{19}$$

where θ_0 is chosen to yield a 3-dB beamwidth of 12°, and G_0 represents the maximum gain, set to 21 dBi.

Figure 11 shows the capacity of the patch antenna array in a ULA setup, where beam-steering is achieved by adjusting the phases at each element. The center frequency f_0 is set to 140 GHz, and the antenna spacing is of $s = \lambda_0/2$. Each point in the plot indicates the achievable capacity if the array steers in that direction (θ_s). The array factor is modeled following [46] as

$$G_{\text{Array}} = \frac{\sin^2\left[N\pi s(\sin\theta/\lambda - \sin\theta_s/\lambda_0)\right]}{N\sin^2\left[\pi s(\sin\theta/\lambda - \sin\theta_s/\lambda_0)\right]}, \tag{20}$$

which accounts for the beam squint effect, a phenomenon typically observed in wideband beamforming antenna arrays. Beam squint refers to the frequency-dependent change in the direction of the radiated or received beam. It arises because the phase shifts applied to each antenna element are optimized for a specific center frequency. When the operating frequency deviates from this center frequency, the phase shifts no longer align with the intended beam direction, causing the beam's pointing angle to shift. This effect ultimately limits the usable bandwidth of the array.

For patch antennas, the gain is given by

$$G_{\text{Patch}} = G_0 \text{sinc}^2\left[\frac{\pi W}{\lambda}\sin\theta\right]\cos^2\left[\frac{\pi L}{\lambda}\sin\theta\right], \tag{21}$$

where G_0 is set to 6 dBi in this case. The length (L) and width (W) of each patch antenna are both $\lambda_0/2$.

Finally, to model the total gain, the contributions from both the patch antenna gain and the array factor are combined

$$G_{\text{Total}} = G_{\text{Patch}} G_{\text{Array}}. \tag{22}$$

To compare these solutions, Figure 12 illustrates the capacity at a fixed distance of 1 m, showing how it changes as a function of the propagation angle at which the array is transmitting.

The results highlight the distinct characteristics of the evaluated antenna systems. Horn antennas, while providing high gain, their narrow beams limit steering capability unless mechanical steering is employed, which adds complexity. Beamforming phased arrays offer high dynamism through electronic beam-steering but face significant challenges at (sub-)THz frequencies due to hardware complexities, phase-shifter losses, and the beam squint effect, which limits usable transmitted bandwidth.

The tilted LWA array offers a middle ground between these systems. Its relatively high gain ensures good directivity, while its frequency-dependent steering capability introduces the necessary dynamism. Unlike single LWAs or non-tilted LWA arrays, which are limited by restricted usable bandwidth, introducing a tilt enhances the effective bandwidth, enabling achievable capacities on par with conventional architectures. Additionally, the concept of beam squint becomes obsolete, as the frequency dependency of the radiation pattern becomes an advantage that increases effective bandwidth and overall system performance.

Additionally, phased arrays or antennas utilizing phase shifters also contend significant losses. Typical loss values range from 2–6 dB at sub-THz frequencies and 4–10 dB at THz frequencies [24], further highlighting the benefits of alternative approaches like the tilted LWA array.

V. EXPERIMENTAL IMPLEMENTATION AND VALIDATION

To validate the performance of our proposed tilted LWA array for spatial multiplexing in (sub-)THz MIMO systems, we conduct a series of experiments. First, we design and fabricate an optimal rectangular waveguide LWA for use in the LWA array. Then, we evaluate the antenna's performance through real-world measurements, confirming its directivity and steering capabilities. Subsequently, we test the MIMO performance of the tilted LWA array compared to a non-tilted LWA array, assessing each's ability to implement space-time coding (STC) schemes and to transmit multiple independent data streams with minimal interference. These experiments validate our theoretical findings and demonstrate

the practicality of using tilted LWA arrays in (sub-)THz MIMO applications.

A. DESIGN AND VALIDATION OF LEAKY-WAVE ANTENNA

1) LEAKY-WAVE ANTENNA DESIGN

The rectangular waveguide LWA shown in Figure 1 consists of an empty rectangular waveguide with a longitudinal slit in the narrow wall. The parameter values in the image are chosen with the objective of achieving high directivity and sufficient steering range within the specified frequency range. The design is tailored to match the WR6.5 waveguide output of the upconverter, with dimensions of 1.651 mm in width (a) and 0.8255 mm in height (b). The slit has a length L of 30 mm and a width W of 0.2 mm.

The design and performance of the antenna is validated using EM simulations with FEKO software. The far-field is calculated, and the gain of the LWA at different frequencies is shown in Figure 13. The results match expectations, though a significant sidelobe is present around $\theta = 15°$. The gain of the antenna ranges between 12 dBi and 18 dBi as the frequency increases.

The antenna was sent for manufacturing, constructed from brass, and subsequently gold-plated. A visual reference of the antenna size is provided in Figure 14 alongside a quarter.

2) EXPERIMENTAL SETUP

The fabricated LWAs are tested using a Virginia Diodes upconverter and power meter. The LWAs are mounted on the transmitter front-end. A Keysight Performance Signal Generator (PSG) E8257 generates a continuous sinusoid ranging between 119 GHz and 169 GHz, while a second PSG generates the Intermediate Frequency (IF) signal at 1 GHz. This configuration resulted in sinusoids between 120 GHz and 170 GHz, transmitted with a frequency step of 1 GHz. The front-end is mounted on a rotary table to perform measurements on the forward quadrant of the LWA, i.e., from $\theta = 0°$ to $\theta = 90°$ in 1° increments. On the receiver side, positioned 1 m away, a PM5B - VDI/Erickson Power Meter is used, capable of measuring power ranges from 1 μW to 200 mW. The power meter input port is connected to a lens horn antenna with a gain of 38-41 dBi. The rotary table, PSG, and power meter are controlled using MATLAB. Measurements of the received power are taken, allowing sufficient time for the power meter to stabilize.

3) EXPERIMENTAL RESULTS

The gain of the LWA is determined using a link budget analysis, where all terms are expressed in decibels (dB):

$$G_T = P_R - P_T - G_R - L_{spr} - L_{abs}, \tag{23}$$

where G_T and G_R are the gains of the transmit and receive antennas, respectively; P_T is the output transmit power of the test bed; $L_{spr} = 32.4478 + 20\log_{10}(fd)$ is the spreading loss, with f and d being the frequency and distance, respectively;

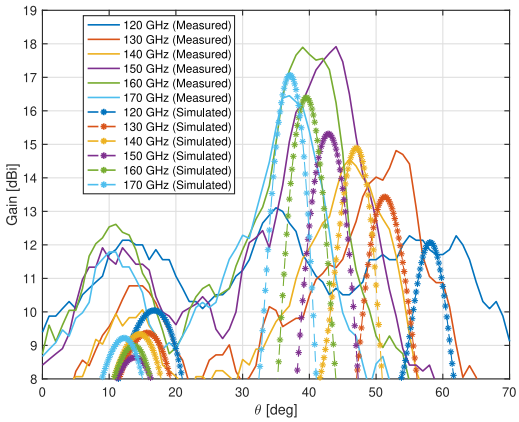

FIGURE 13. Measured and simulated radiation pattern of the LWA.

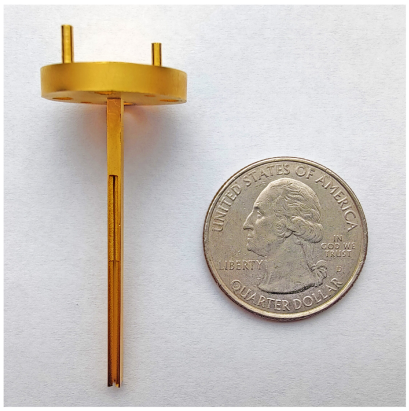

FIGURE 14. Visualization of the fabricated LWA alongside a quarter.

and $L_{abs} = 4.3429kd$ is the atmospheric absorption loss, with k representing the molecular absorption coefficient. All these parameters are frequency-dependent.

After performing the calculations, the gain of the LWA was determined, as shown in Figure 13. The measured values closely match those obtained from the EM simulations, with the gain increasing from approximately 12 dBi to 18 dBi as the frequency increases. As is typical for uniform LWAs, their performance when radiating near the broadside direction is poor, with correct behavior observed only above 125 GHz. Moreover, the gain does not increase with frequency as smoothly as predicted by the simulations, and the beamwidth is larger than expected. These differences are probably due to fabrication tolerances. Accurately determining the frequency response of all hardware components is also very challenging, so the link budget analysis cannot provide precise real values.

Future work could investigate alternative LWA designs to achieve a broader steerability range and enhanced gain near the broadside direction. Conducting tests in an anechoic chamber could further enhance measurement accuracy. Lastly, employing finer fabrication tolerances could improve overall efficiency. Despite these limitations, the gain remains relatively high, the steering angle aligns with expectations,

(a) (b)

FIGURE 15. Experimental setup: (a) 2×2 MIMO system, (b) tilted LWA array in the transmitter side.

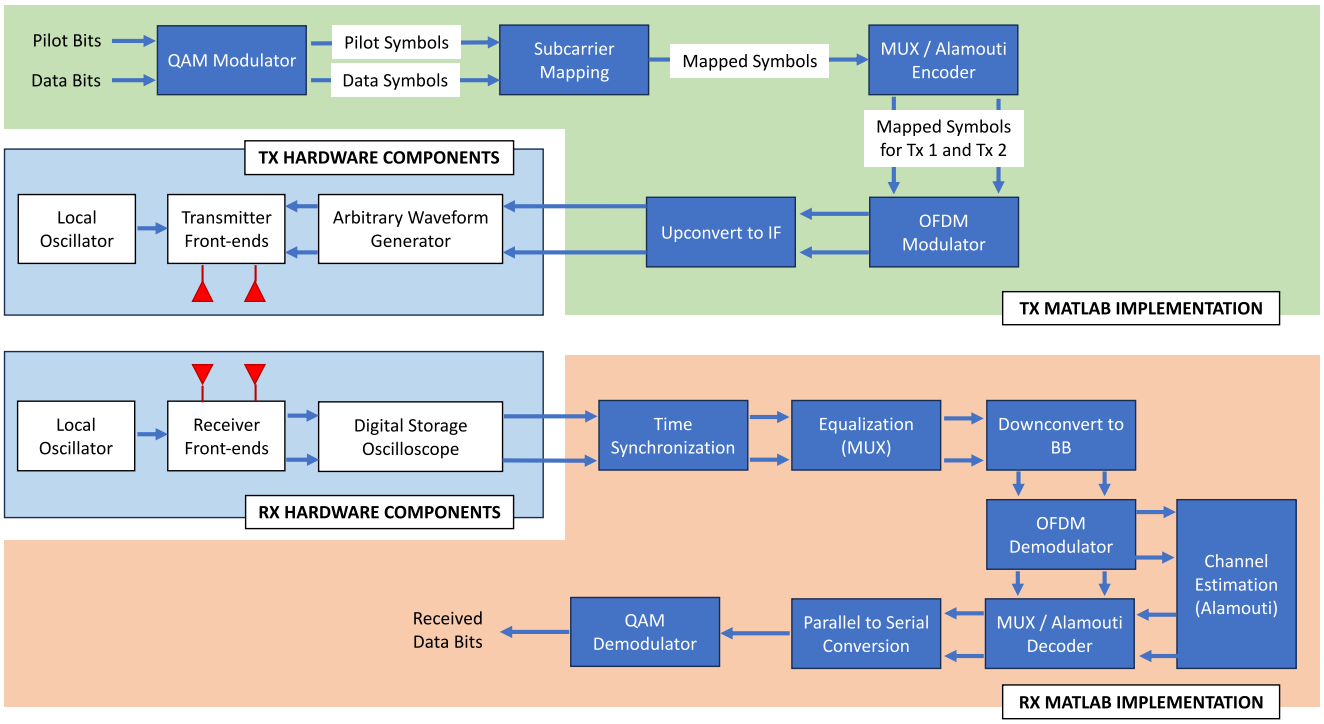

FIGURE 16. System block diagram.

and the results are sufficient to support the experimental analysis in the following section.

B. IMPLEMENTING MIMO TECHNIQUES WITH A LEAKY-WAVE ANTENNA ARRAY

1) EXPERIMENTAL SETUP

To evaluate the capabilities of the LWA array, we implement two distinct MIMO techniques: the Alamouti scheme [47] and spatial multiplexing. The Alamouti scheme, a form of STC, leverages spatial diversity to enhance signal robustness and reliability by transmitting duplicate signals across separate antennas, thus facilitating effective signal reception. Our goal was to assess the performance of the LWA array with various tilting angles using both MIMO techniques. By tilting the LWAs, we aim to transmit separate data streams with minimal interference, enabling spatial multiplexing based solely on the antenna's radiation pattern. The Alamouti scheme served as a benchmark for comparison due to its established reliability.

We leverage the TeraNova testbed [48] in a 2×2 fully connected MIMO architecture. The experimental setup is depicted in Figure 15. We use a center frequency of 147.5 GHz, with the LWA transmitting around $\theta = 45°$. The LWAs are mounted on the transmitter front-ends one on top of the other at the designated tilt angle, with about 5 cm of vertical separation between them. The receivers are positioned 60 cm away. Each receiver is placed at a 45° angle relative to each transmitter, so as the LWA tilting angle

increases, the angular separation between the receivers also increases. For the case where the tilting angle is 0°, the two receivers are also mounted one on top of the other.

The system block diagram is shown in Figure 16. On the transmitter side, the digitally created waveform is converted to analog using a high-speed Digital-to-Analog Converter (DAC) in the Arbitrary Waveform Generator (AWG) M8196A. This analog IF signal is mixed with the Local Oscillator (LO) signal, initially generated by the same PSG at baseband and brought to the Radio Frequency (RF) by two frequency doublers. The mixed signal is then amplified and radiated out of the antenna. On the receiver side, the incoming high-frequency signal is down-converted to an IF signal and captured by a Keysight Digital Storage Oscilloscope (DSO) Z632A. The DSO, equipped with an Analog-to-Digital Converter (ADC), converts the analog IF signal into a digital format for further processing.

The signal modulation and demodulation are performed in MATLAB. Given the highly frequency-selective channel characteristics and our broadband signal, we choose an Orthogonal Frequency Division Multiplexing (OFDM) waveform to allow for better manipulation and decoding in the frequency domain.

We test both Alamouti and spatial multiplexing MIMO techniques. The encoder separates the signal into two streams. For Alamouti, these streams consist of the same signal, providing spatial diversity, while for spatial multiplexing, the streams consist of two independent signals, each sent through one transmit antenna. At the decoder, the signals are appropriately recombined.

We evaluate the impact of different bandwidths (2.5, 5, and 10 GHz) on signal quality and data rates for each MIMO technique. This helps to determine the performance and effectiveness of Alamouti and spatial multiplexing under varying bandwidth conditions.

For the physical layer, data bits are organized into a frame. The frame began with an 18-bit Maximum Length Sequence (MLS) modulated using Binary Phase-Shift Keying (BPSK) for time synchronization, used by both transmitters. After the header, the rest of the frame is modulated using the MIMO OFDM scheme. For channel equalization, during the first portion of the frame all subcarriers are used to send pilot bits and the latter part of the frame all are used to send data bits as in [17]. We use a Quadrature Amplitude Modulation (QAM) scheme on each subcarrier and test both 4QAM and 16QAM modulation orders. In our experiments, we use 8, 16, and 32 OFDM symbols for the pilot for the 2.5, 5, and 10 GHz bandwidths, respectively, and 40, 80, and 160 OFDM symbols for the data portion of the frame for the same bandwidths, ensuring that the generated signals have the same duration in time for fair comparison. Additionally, we include a 10% cyclic prefix to eliminate inter-symbol interference.

At the receiver, after removing the cyclic prefix and demodulating the OFDM symbols to baseband, we perform channel estimation using a scaled least squares (SLS) algorithm [49] on the received pilot symbols. We use $\gamma_0 = \frac{1}{tr(R_H)}$ as our scaling factor for the SLS estimate, where $R_H = H_{LS}^H H_{LS}$ is the correlation matrix of the least squares (LS) estimate, $tr(.)$ indicates the trace of a matrix, and $(.)^H$ is the conjugate transpose of a matrix.

2) EXPERIMENTAL RESULTS

As mentioned, we transmit multiple waveforms using the two MIMO techniques: spatial multiplexing and Alamouti STC. Our objective is to determine if it is possible to send two data streams simultaneously without significantly affecting the quality of the received signal. The resulting data rate, Error Vector Magnitude (EVM), and Bit Error Rate (BER) for each case are presented in Figure 17.

The results confirm our theoretical findings from Section IV. First, we observe that applying a tilt to the LWA array elements benefits spatial multiplexing. The BER and EVM significantly decrease compared with the non-tilted array in this case. The tilting angle of 20° allows to have minimal co-propagation interference, though a 10° also provides acceptable results. Conversely, using a non-tilted array yields better BER and EVM in the case of the Alamouti scheme.

However, if comparing between waveforms with equal data rate, the spatial multiplexing can actually provide a better BER and EVM. For example, if we compare the cases that provides a data rate of 26.9 Gbps, the spatial multiplexing with 10 GHz of bandwidth and 4QAM with a tilting angle of 20° has better BER and EVM than the Alamouti case with 10 GHz bandwidth, 16QAM and a tilting angle of 0°. Same results can be seen when comparing the results with data rates of 13.45 Gbps and 6.72 Gbps. The reason behind this is because with spatial multiplexing there is a larger margin for error, as it requires less bandwidth or modulation scheme to achieve the same data rate. In general, it seems that utilizing more bandwidth instead of a higher modulation scheme provides better results for a fixed data rate. The BER and EVM are better for both spatial multiplexing and Alamouti in these cases. Examples of the received constellations for a fixed data rate of 13.45 Gbps are shown in Figure 18.

In this lab setup, the receivers are positioned at specific angles, and the appropriate frequency band is selected based on the expected radiation pattern of the LWAs. In real-world applications, channel knowledge at the transmitter and the water-filling algorithm would be employed to maximize data rates in dynamic scenarios. The advantage of the proposed array lies in its ability to achieve spatial multiplexing with angular resolution, thereby minimizing the need for extensive channel information and reducing the signal processing requirements compared to conventional SVD methods used in standard MIMO spatial multiplexing. Tilted LWAs can simultaneously transmit distinct signals to their respective receivers with minimal co-propagation interference, inherently facilitating spatial multiplexing.

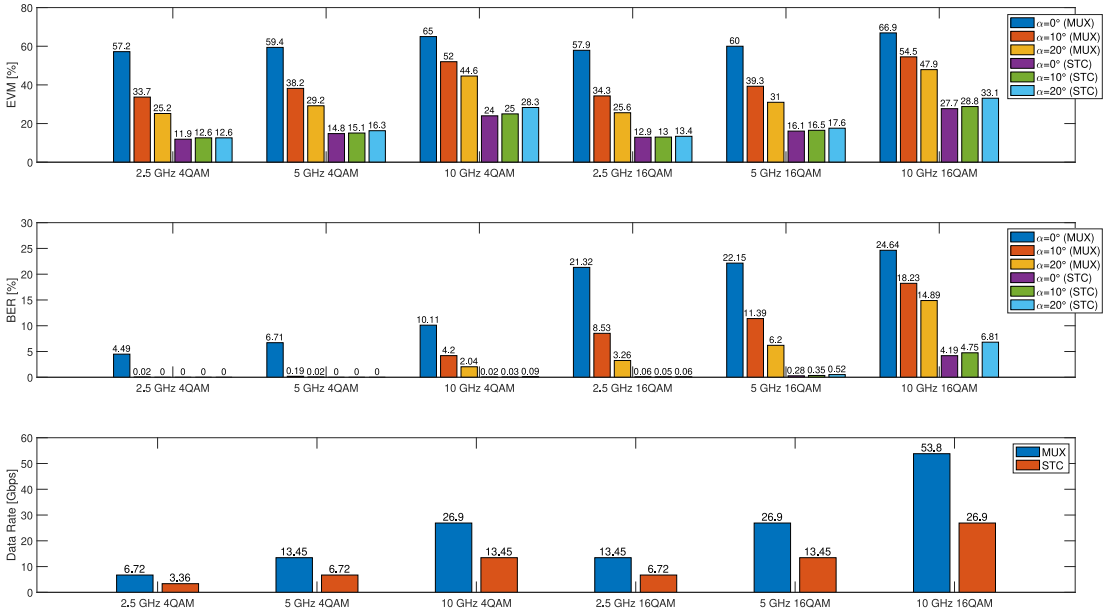

FIGURE 17. Experimental results showing the EVM, BER, and data rates for spatial multiplexing (MUX) and Alamouti space-time coding (STC) across different bandwidths, modulation schemes, and tilting angles.

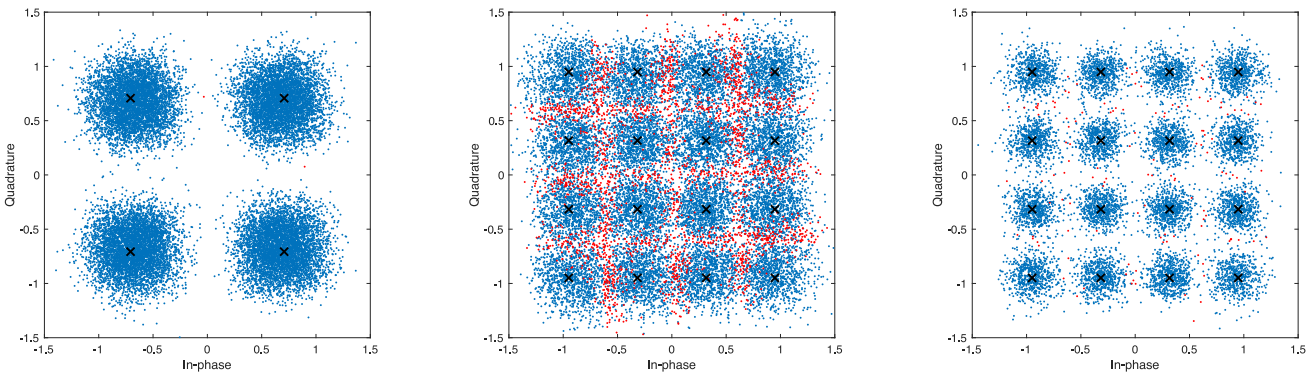

(a) MUX – 5 GHz, 4QAM, $\alpha = 20°$ (b) MUX – 2.5 GHz, 16QAM, $\alpha = 20°$ (c) STC – 5 GHz, 16QAM, $\alpha = 0°$

FIGURE 18. Example of received constellations with fixed data rate of 13.45 Gbps.

VI. CHALLENGES AND FUTURE WORK

While the proposed tilted LWA array architecture offers significant promise for enabling spatial multiplexing in (sub-)THz MIMO systems, several challenges must be addressed before practical deployment. One of the main issues involves **frequency allocation and channel estimation.** The inherent frequency-dependent propagation of LWAs demands precise frequency planning to ensure reliable links at the correct angles. OFDM emerges as a particularly effective solution because it subdivides the available bandwidth into subcarriers that can be individually mapped to specific angles. However, successfully leveraging OFDM in this context depends on obtaining accurate CSI at the transmitter, which can be achieved through channel discovery techniques developed for LWAs, as explored in prior research [21], [22].

Although waterfilling algorithms can theoretically yield optimal power allocation, they are often computationally intensive. Thus, a simpler and more feasible approach is to assign uniform power distribution across selected subcarriers, as done in our experimental demonstration. Furthermore, in multiuser environments, preserving stable connections becomes more challenging as users traverse different parts of the coverage area. The system must dynamically reallocate both frequency and power in response to changing spatial and temporal user requirements. Looking ahead, developing adaptive algorithms that capitalize on the unique properties of LWAs to manage frequency and power allocation in real time will be essential, particularly in balancing performance with computational complexity.

We also evaluated the performance of a staircase LWA array, composed of multiple LWAs stacked in a stepped

arrangement to achieve 360° angular coverage. This architecture serves as an alternative AP architecture that offers high directivity and adaptability due to the intrinsic properties of LWAs. Nonetheless, certain challenges need to be addressed. Deploying a large number of LWAs requires additional RF chains, which could increase costs. This issue can be mitigated by designing LWAs with broader beam-steering ranges to reduce the number of antennas needed for full coverage. Additionally, **developing a compact configuration that accommodates many LWAs** in a small volume is essential. Despite their length, the narrow profile of LWAs, specially at these high frequencies, makes a compact AP design feasible. This approach offers a practical and efficient solution for advanced communication systems.

Blockage is another major hurdle for any LoS-based MIMO systems at THz frequencies, as it can drastically reduce link reliability. Common mitigation strategies include deploying multiple APs or introducing RIS to improve coverage. Meanwhile, **interference**–a core issue in most wireless systems–is partially mitigated here by the high directivity of LWAs. In downlink scenarios, beams are narrowly focused on the intended user, thereby reducing interference to others; in uplink scenarios, the same directivity also helps filter out unwanted signals.

Beyond these communication-related considerations, several **fabrication and integration challenges** remain. Scaling the number of LWAs while preserving structural integrity is crucial to achieving compact, high-performance solutions. In our laboratory demonstration, each front end was simply placed atop another to validate the concept. Fabricating a suitable casing or feeding network that can reliably feed each LWA while maintaining structural integrity would enable greater scalability and integration. Additionally, new antenna designs may unlock further possibilities. For instance, filling the LWA with dielectric material could expand the beam-steering range utilizing a narrower bandwidth [18], so that steerability could be performed in more practical systems. Overcoming these technical hurdles will be critical for transforming tilted LWA arrays into a viable, high-capacity option for next-generation (sub-)THz MIMO systems.

Additionally, the **near-field effects** of the antenna must be considered, as they depend on the specific LWA design and operating frequency. In our design, the near-to-far field boundary was determined to be approximately 16 cm, ensuring operation within the far field. However, as operating frequencies increase or larger LWA designs relative to the wavelength are utilized, thorough consideration of the near-field region becomes crucial.

VII. CONCLUSION

In this paper, we have proposed the use of LWAs in (sub-)THz MIMO systems, demonstrating that their high directivity and frequency-dependent beam-steering capabilities offer significant advantages. We have introduced a novel approach of tilting the elements of an LWA array to enable spatial multiplexing based solely on their characteristic radiation pattern. This approach optimizes bandwidth utilization of the LWAs and enhances spectral efficiency, facilitating LWA-based communications with improved data rates. Numerical analyses demonstrated that spatial multiplexing with a tilted LWA array outperforms combining under specific conditions and illustrated how the multiplexing capabilities scale with the number of LWAs. Our findings confirm that LWAs can support high data rates owing to their directive radiation pattern and beam-steering features. Additionally, we examined the performance of a staircase LWA array as an AP in a multiuser environment, showing its ability to exploit user diversity through spatial multiplexing. We also compared the performance of the tilted LWA array with other antenna array technologies, providing insights into its advantages and trade-offs. Experimentally, we have provided the first implementation of a sub-THz MIMO system using an LWA array, validating the performance of the tilted configuration. The results align with our theoretical predictions, showcasing promising data rates with acceptable EVM and BER in a lab setup. Finally, we discussed challenges and future work to address practical implementation in real-world scenarios. We hope this work contributes to further research and development in (sub-)THz MIMO systems.

REFERENCES

[1] I. F. Akyildiz, C. Han, Z. Hu, S. Nie, and J. M. Jornet, "Terahertz band communication: An old problem revisited and research directions for the next decade," *IEEE Trans. Commun.*, vol. 70, no. 6, pp. 4250–4285, Jun. 2022.

[2] M. Polese et al., "Coexistence and spectrum sharing above 100 GHz," *Proc. IEEE*, vol. 111, no. 8, pp. 928–954, Aug. 2023.

[3] C. Lin and G. Y. L. Li, "Terahertz communications: An array-of-subarrays solution," *IEEE Commun. Mag.*, vol. 54, no. 12, pp. 124–131, Dec. 2016.

[4] C. Han, L. Yan, and J. Yuan, "Hybrid beamforming for terahertz wireless communications: Challenges, architectures, and open problems," *IEEE Wireless Commun.*, vol. 28, no. 4, pp. 198–204, Aug. 2021.

[5] A. Faisal, H. Sarieddeen, H. Dahrouj, T. Y. Al-Naffouri, and M.-S. Alouini, "Ultramassive MIMO systems at terahertz bands: Prospects and challenges," *IEEE Veh. Technol. Mag.*, vol. 15, no. 4, pp. 33–42, Dec. 2020.

[6] B. Ning et al., "Beamforming technologies for ultra-massive MIMO in terahertz communications," *IEEE Open J. Commun. Soc.*, vol. 4, pp. 614–658, 2023.

[7] S. Ju and T. S. Rappaport, "Sub-terahertz spatial statistical MIMO channel model for urban microcells at 142 GHz," in *Proc. IEEE Global Commun. Conf. (GLOBECOM)*, Madrid, Spain, Dec. 2021, pp. 1–6.

[8] Y. Xing and T. S. Rappaport, "Propagation measurements and path loss models for sub-THz in urban microcells," in *Proc. IEEE Int. Conf. Commun.*, Montreal, QC, Canada, Jun. 2021, pp. 1–6.

[9] H. Do, S. Cho, J. Park, H.-J. Song, N. Lee, and A. Lozano, "Terahertz line-of-sight MIMO communication: Theory and practical challenges," *IEEE Commun. Mag.*, vol. 59, no. 3, pp. 104–109, Mar. 2021.

[10] N. Maletic, D. L. Lopacinski, M. Goodarzi, D. M. Eissa, and D. J. Gutiérrez, "A study of LOS MIMO for short-range sub-THz wireless links," in *Proc. Mobile Commun., Technol. Appl., 25th ITG-Symp.*, 2021, pp. 1–6.

[11] I. F. Akyildiz and J. M. Jornet, "Realizing ultra-massive MIMO (1024 × 1024) communication in the (0.06–10) terahertz band," *Nano Commun. Netw.*, vol. 8, pp. 46–54, Jun. 2016.

[12] A. A. Farid, A. S. H. Ahmed, A. Dhananjay, P. Skrimponis, S. Rangan, and M. Rodwell, "135GHz CMOS / LTCC MIMO receiver array tile modules," in *Proc. IEEE BiCMOS Compd. Semicond. Integr. Circuits Technol. Symp. (BCICTS)*, Monterey, CA, USA, Dec. 2021, pp. 1–4.

[13] S. Abu-Surra et al., "End-to-end 140 GHz wireless link demonstration with fully-digital beamformed system," in *Proc. IEEE Int. Conf. Commun. Workshops (ICC Workshops)*, Montreal, QC, Canada, Jun. 2021, pp. 1–6.

[14] C. Castro, R. Elschner, T. Merkle, and C. Schubert, "100 Gbit/s terahertz-wireless real-time transmission using a broadband digital-coherent modem," in *Proc. IEEE 2nd 5G World Forum (5GWF)*, Sep. 2019, pp. 399–402.

[15] H. Zhou "Utilizing multiplexing of structured THz beams carrying orbital-angular-momentum for high-capacity communications," *Opt. Exp.*, vol. 30, no. 14, Jul. 2022, Art. no. 25418.

[16] H. Zhao, B. Quan, X. Wang, C. Gu, J. Li, and Y. Zhang, "Demonstration of orbital angular momentum multiplexing and demultiplexing based on a metasurface in the terahertz band," *ACS Photon.*, vol. 5, no. 5, pp. 1726–1732, May 2018.

[17] D. M. Bodet and J. M. Jornet, "Directional antennas for sub-THz and THz MIMO systems: Bridging the gap between theory and implementation," *IEEE Open J. Commun. Soc.*, vol. 4, pp. 2261–2273, 2023.

[18] R. Johnson and H. Jasik, *Antenna Engineering Handbook* (Electronics Electrical Engineering). New York, NY, USA: McGraw-Hill, 1993.

[19] N. J. Karl, R. W. McKinney, Y. Monnai, R. Mendis, and D. M. Mittleman, "Frequency-division multiplexing in the terahertz range using a leaky-wave antenna," *Nat. Photon.*, vol. 9, no. 11, pp. 717–720, Nov. 2015.

[20] P. Lu et al., "Mobile THz communications using photonic assisted beam steering leaky-wave antennas," *Opt. Expr.*, vol. 29, no. 14, pp. 21629–21638, Jul. 2021.

[21] B. Husain, M. Steeg, and A. Stöhr, "Estimating direction-of-arrival in a 5G hot-spot scenario using a 60 GHz leaky-wave antenna," in *Proc. IEEE Int. Conf. Microw., Antennas, Commun. Electron. Syst. (COMCAS)*, Nov. 2017, pp. 1–4.

[22] Y. Ghasempour, C.-Y. Yeh, R. Shrestha, D. Mittleman, and E. Knightly, "Single shot single antenna path discovery in THz networks," in *Proc. 26th Annu. Int. Conf. Mobile Comput. Netw.*, Apr. 2020, pp. 1–13.

[23] A. D. Comas, D. Bodet, Z. Fang, H. Guerboukha, D. M. Mittleman, and J. M. Jornet, "MIMO spatial multiplexing with an array of tilted leaky-wave antennas for terahertz communications," in *Proc. IEEE Future Netw. World Forum (FNWF)*, Baltimore, MD, USA, Nov. 2023, pp. 1–8.

[24] K. Rasilainen, T. D. Phan, M. Berg, A. Pärssinen, and P. J. Soh, "Hardware aspects of sub-THz antennas and reconfigurable intelligent surfaces for 6G communications," *IEEE J. Sel. Areas Commun.*, vol. 41, no. 8, pp. 2530–2546, Aug. 2023.

[25] X. Chen, N. M. Monroe, G. C. Dogiamis, R. A. Stingel, P. Myers, and R. Han, "A 265-GHz CMOS reflectarray with 98×98 elements for 1°-wide beam forming and high-angular-resolution radar imaging," *IEEE J. Solid-State Circuits*, vol. 59, no. 11, pp. 3655–3669, Nov. 2024.

[26] S. Venkatesh, X. Lu, H. Saeidi, and K. Sengupta, "A high-speed programmable and scalable terahertz holographic metasurface based on tiled CMOS chips," *Nat. Electron*, vol. 3, no. 12, pp. 785–793, Dec. 2020.

[27] M. Tamagnone et al., "Graphene reflectarray metasurface for terahertz beam steering and phase modulation," Jun. 2018, *arXiv:1806.02202*.

[28] L. Dai et al., "Reconfigurable intelligent surface-based wireless communications: Antenna design, prototyping, and experimental results," *IEEE Access*, vol. 8, pp. 45913–45923, 2020.

[29] W. Tang et al., "Wireless communications with reconfigurable intelligent surface: Path loss modeling and experimental measurement," *IEEE Trans. Wireless Commun.*, vol. 20, no. 1, pp. 421–439, Jan. 2021.

[30] Y. Yang, O. D. Gurbuz, and G. M. Rebeiz, "An eight-element 370–410-GHz phased-array transmitter in 45-nm CMOS SOI with peak EIRP of 8–8.5 dBm," *IEEE Trans. Microw. Theory Techn.*, vol. 64, no. 12, pp. 4241–4249, Dec. 2016.

[31] D. Headland, W. Withayachumnankul, M. Fujita, and T. Nagatsuma, "Integrated luneburg and maxwell fisheye lenses for the terahertz range," in *Proc. 44th Int. Conf. Infrared, Millim., THz Waves (IRMMW-THz)*, 2019, pp. 1–2.

[32] C.-Y. Yeh, Y. Ghasempour, Y. Amarasinghe, D. M. Mittleman, and E. W. Knightly, "Security in terahertz WLANs with Leaky wave antennas," in *Proc. 13th ACM Conf. Secur. Privacy Wireless Mobile Netw.*, Jul. 2020, pp. 317–327.

[33] H. Guerboukha et al., "Efficient leaky-wave antennas at terahertz frequencies generating highly directional beams," *Appl. Phys. Lett.*, vol. 117, no. 26, Dec. 2020, Ar. no. 261103.

[34] H. Matsumoto, I. Watanabe, A. Kasamatsu, and Y. Monnai, "Integrated terahertz radar based on leaky-wave coherence tomography," *Nat. Electron.*, vol. 3, no. 2, pp. 122–129, Feb. 2020.

[35] P. Lu et al., "InP-based THz beam steering leaky-wave antenna," *IEEE Trans. THz Sci. Technol.*, vol. 11, no. 2, pp. 218–230, Mar. 2021.

[36] K. Murano et al., "Low-profile terahertz radar based on broadband leaky-wave beam steering," *IEEE Trans. THz Sci. Technol.*, vol. 7, no. 1, pp. 60–69, Jan. 2017.

[37] M. Esquius-Morote, J. S. Gómez-Dı'az, and J. Perruisseau-Carrier, "Sinusoidally modulated graphene leaky-wave antenna for electronic beamscanning at THz," *IEEE Trans. THz Sci. Technol.*, vol. 4, no. 1, pp. 116–122, Jan. 2014.

[38] X.-C. Wang, W.-S. Zhao, J. Hu, and W.-Y. Yin, "Reconfigurable terahertz leaky-wave antenna using graphene-based high-impedance surface," *IEEE Trans. Nanotechnol.*, vol. 14, no. 1, pp. 62–69, Jan. 2015.

[39] W. Fuscaldo, P. Burghignoli, P. Baccarelli, and A. Galli, "A reconfigurable substrate–superstrate graphene-based leaky-wave THz antenna," *IEEE Antennas Wireless Propag. Lett.*, vol. 15, pp. 1545–1548, 2016.

[40] W. Fuscaldo et al., "A reconfigurable multilayered THz leaky-wave antenna employing liquid crystals," in *Proc. 11th Eur. Conf. Antennas Propag. (EUCAP)*, Mar. 2017, pp. 849–851.

[41] S. A. Busari et al., "Generalized hybrid beamforming for vehicular connectivity using THz massive MIMO," *IEEE Trans. Veh. Technol.*, vol. 68, no. 9, pp. 8372–8383, Sep. 2019.

[42] H. Sarieddeen, M.-S. Alouini, and T. Y. Al-Naffouri, "Terahertz-band ultra-massive spatial modulation MIMO," *IEEE J. Sel. Areas Commun.*, vol. 37, no. 9, pp. 2040–2052, Sep. 2019.

[43] S. Park, A. Alkhateeb, and R. W. Heath, "Dynamic subarrays for hybrid precoding in wideband mmWave MIMO systems," *IEEE Trans. Wireless Commun.*, vol. 16, no. 5, pp. 2907–2920, May 2017.

[44] J.-F. Frigon, C. Caloz, and Y. Zhao, "Dynamic radiation pattern diversity (DRPD) MIMO using CRLH leaky-wave antennas," in *Proc. IEEE Radio Wireless Symp.*, Orlando, FL, USA, Jan. 2008, pp. 635–638.

[45] D. Tse and P. Viswanath, *Fundamentals of Wireless Communication*, 1st ed. Cambridge, U.K.: Cambridge Univ., May 2005.

[46] M. Longbrake, "True time-delay beamsteering for radar," in *Proc. IEEE Nat. Aerosp. Electron. Conf. (NAECON)*, 2012, pp. 246–249.

[47] S. Alamouti, "A simple transmit diversity technique for wireless communications," *IEEE J. Sel. Areas Commun.*, vol. 16, no. 8, pp. 1451–1458, Oct. 1998.

[48] P. Sen, D. A. Pados, S. N. Batalama, E. Einarsson, J. P. Bird, and J. M. Jornet, "The TeraNova platform: An integrated testbed for ultra-broadband wireless communications at true terahertz frequencies," *Comput. Netw.*, vol. 179, Oct. 2020, Art. no. 107370.

[49] M. Biguesh and A. Gershman, "MIMO channel estimation: Optimal training and tradeoffs between estimation techniques," in *Proc. IEEE Int. Conf. Commun.*, vol. 5, Paris, France, 2004, pp. 2658–2662.